Modelling and defect size estimation of a defective bearing

Francesco Larizza (1), Carl Q. Howard (1), Steven Grainger (1) and Wenyi Wang (2)

(1) School of Mechanical Engineering, The University of Adelaide, Adelaide, Australia
(2) DST Group, Victoria, Australia

ABSTRACT

Rolling element bearings eventually become worn and fail by developing surface defects, such as spalls, dents, and pits. Previous researchers have tested bearings with defects that have sharp 90° rectangular edges that were used to develop analytical models of a defective bearing and defect size estimation methods. These models have limitations that require smooth surfaces and constant curvature of the bearing components; as well as assuming the defect profile. An analytical model has been developed for a rolling element bearing that uses a measured defect profile and removes the limitations of previous analytical models that use analytical expressions for contact area and force. The predicted vibration response of a bearing with a defect on the outer raceway was compared with experimental results. It was found that the new analytical model was able to predict the vibration response of a defective bearing. Current defect size estimation methods that use time-series data to estimate the size; these methods do have an aliasing issue when the defect is larger than the separation angle of the rolling elements. In this paper a method for determining if the length of a spall defect is greater than the separation angle of the rolling elements using the varying stiffness of the bearing assembly is presented. The developed model and experimental data have been made publicly available.

1 INTRODUCTION

Bearings in a machine will eventually fail, and the most common reason for failure is the formation of surface defects from the propagation of fatigue cracks or the removal of surface grains during operation. These defects occur due to insufficient lubrication and high contact stresses between the rolling element and the raceway of the bearing, causing spalls, dents, and pits to form on the contact surfaces. These defects cause the applied load on the rolling element to differ, causing the relative distance from the cup to cone to vary from normal, resulting in higher than normal vibration amplitudes. The condition of a defective bearing can be determined by analysing this vibration response, which can be used for scheduling maintenance actions.

Previous studies on the vibration signature of a bearing with a sharp rectangular raceway defect found that as the rolling element traverses the defect, the resultant vibration response has two distinct features. The first is a low-frequency component that is caused by the rolling element entering and exiting the defect and the second is a high-frequency component, which is caused by the rolling element striking the trailing edge of the defect (Sawalhi and Randall 2008a). The time between these two events has been used to estimate the size of the defect, but have been shown to be inaccurate as the load and shaft speed increase (Sawalhi and Randall 2011). An aliasing issue is also present if the defect is greater than the separation angle of the rolling elements as the vibration response in the time-domain is similar to a smaller line spall defect (Petersen, Howard, and Prime 2015).

This research presents a model that removes some of the assumptions made by previous researchers (Moazen-Ahmadi, Petersen, and Howard 2015), and uses a measured defect profile in the model to predict the vibration response of the defective bearing. Finally, the research experimentally shows that the hypothesis presented by Petersen, Howard, and Prime (2015) can be used to determine if a defect is an extended or line spall defect.

2 PREVIOUS WORK

Previous experimental and simulation studies by Epps (1991), Sawalhi and Randall (2011), Moazen-Ahmadi, Petersen, and Howard (2015) and Singh et al. (2013), examined the vibration response of a defective bearing, with sharp 90° rectangular defects. It was found that there are four key vibration signatures as the rolling element traverses the defect. Figure 1 shows a typical vibration response from a defective bearing with a spall defect on the outer raceway. A small negative acceleration occurs when the roller begins to transition into the defect (Event 1), and when the rolling element has completely unloaded a low-frequency response occurs (Event 2). It was also

suggested that the high-frequency event is a result of the rolling element striking the trailing edge of the defect, or for a defect with a large circumferential extent, when the rolling element strikes the bottom of the defect (Event 3). A second low-frequency event occurs as the rolling element begins to reload between the raceways, as it is forced out of the defect (Event 4).

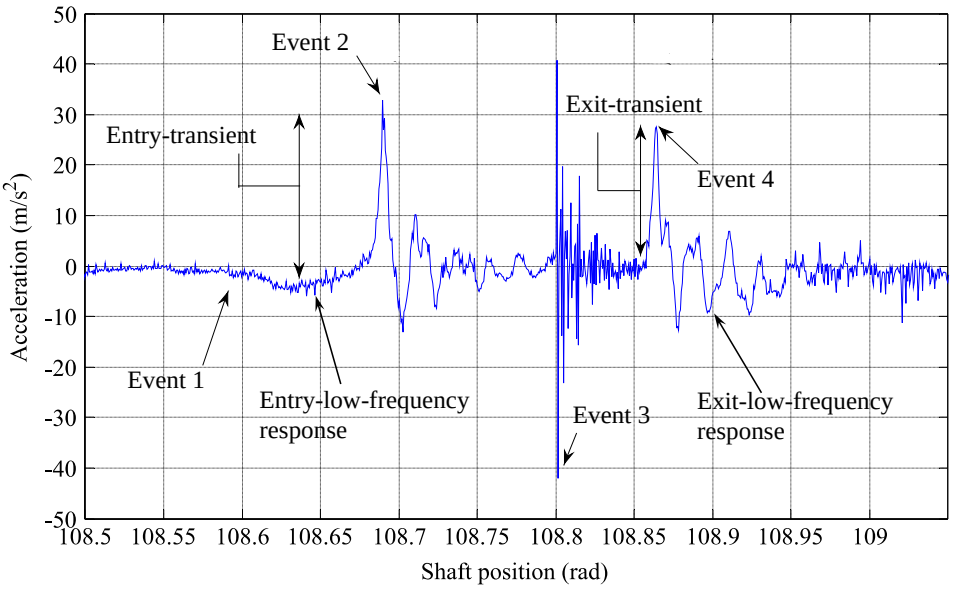

Figure 1: The vibration response of a bearing as a rolling element travels through a rectangular spall defect on the outer ring, showing the low and high-frequency events. Image adapted from Moazen-Ahmadi, Howard, and Petersen (2015).

These relationships between the vibration response and position of the rolling element were derived using multi-body dynamics models (Moazen-Ahmadi, Petersen, and Howard 2015), (Sawalhi and Randall 2008b), (Petersen, Howard, and Prime 2015) and (Choudhury and Tandon 2006), and finite element models (Singh et al. 2014), as it is difficult to image or measure the path of rolling elements in an operational bearing. Work by Yang et al. (2016) and Mirzaei et al. (2008) have measured the path of the rolling elements in an operational bearing using a high-speed camera. The resolution of the presented results was about 20 µm, which is much too large to compare the simulated rolling element path with accuracy. Note that researchers have not experimentally validated the dynamic path of the rollers in a defective bearing. To simplify the analysis of a bearing, the majority of previously proposed multi-body dynamic models included a combination assumptions such as; the rolling elements are considered massless or point masses, slippage of the rollers are ignored, the inertia of the rollers are ignored, the path of the roller is assumed, and others.

Moazen-Ahmadi, Petersen, and Howard (2015) developed a comprehensive model, where the rolling elements were considered to have finite mass and size; and the roller path was not assumed but determined through appropriate physics, such as centripetal acceleration and the change in the contact point as the rolling element transitions into and out of the defect. However, the model has limitations, such as the wavelength of the roughness and the circumferential defect length must be larger than the circumferential contact length. These limitations are a result of the model using Hertzian contact theory to determine the contact forces, which require the contact surfaces to be smooth and continuous. Therefore, when calculating the contact forces on a rough surface, or a surface where the curvature changes rapidly, Hertzian contact theory cannot be used as when a rolling element transitions into and out of the defect, the circumferential contact pressure profile becomes skewed causing the bearing to crush more, and with a rough surface, the contact area is no longer a uniform shape, as some points may not be in contact with the raceway.

Several defect size estimation methods have been suggested previously for bearings with line spall-defects based on detecting the time separation between the entry and exit events from the vibration signal (Sawalhi and Randall

2011). These previous defect size estimation methods underestimate the size of a defect that is larger than, at least, one ball angular spacing. The possibility of using the bearing assembly stiffness variations in defective bearings as a measure to distinguish between extended and line-spall defects was suggested by Petersen, Howard, and Prime (2015), but there was no further investigation. They presented an analytical formulation of the varying static stiffness and load distribution of a ball bearing assembly as a function of the cage angular position. Petersen, Howard, and Prime (2015) analysed the static stiffness variation in defective bearings with rectangular shaped outer raceway defects of varying circumferential extent and similar depths without experimental validation. In the work conducted here, the effects of the applied load on the static stiffness in defective bearings is presented, which was ignored previously.

3 BEARING MODEL

To remove the limitations presented by models that use Hertzian contact theory, a numerical method that uses Love's equation was used to calculate the contact area and contact force of a smooth rolling element on a rough surface. The contact model utilised in the newly developed model does not consider plastic deformation, as this will be used in future work to determine the possible growth of a defect and to reduce the computation time of the contact model. Love's equation allows the discretisation of the contact surface into finite elements and the calculation of the contribution an applied pressure on an element has on the deformation of another element. The discretised surface of a flat plane, where the element size is $2a$ by $2b$ and the rigid body penetration U_z at node z. The rigid body penetration of an element is given by

$$U_z = \sum_{z=1}^{n}\sum_{i=1}^{m}\frac{2p_i(1-\nu^2)}{\pi E}\left[\begin{array}{l}\left((x+a)\,ln\left(\frac{(y+b)+\left((y+b)^2+(x+a)^2\right)^{\frac{1}{2}}}{(y-b)+\left((y-b)^2+(x+a)^2\right)^{\frac{1}{2}}}\right)\right)\\+\left((y+b)\,ln\left(\frac{(x+a)+\left((y+b)^2+(x+a)^2\right)^{\frac{1}{2}}}{(x-a)+\left((y+b)^2+(x-a)^2\right)^{\frac{1}{2}}}\right)\right)\\+\left((x-a)\,ln\left(\frac{(y-b)+\left((y-b)^2+(x-a)^2\right)^{\frac{1}{2}}}{(y+b)+\left((y+b)^2+(x-a)^2\right)^{\frac{1}{2}}}\right)\right)\\+\left((y-b)\,ln\left(\frac{(x-a)+\left((y-b)^2+(x-a)^2\right)^{\frac{1}{2}}}{(x+a)+\left((y-b)^2+(x+a)^2\right)^{\frac{1}{2}}}\right)\right)\end{array}\right] \quad (1)$$

where a is the half element length, b is half the element width, x and y are the distance from node z to p_i in the x and y-direction respectively; p_i is the applied pressure on the element that is contributing to the deformation at z; and ν and E are the Poisson's Ratio and the Young's Modulus of the material, respectively. The distances from node z to p_i in the x and y-directions and the rigid body penetration U_z are given by

$$x = 2a|z_x - i_x| \quad (2)$$

$$y = 2b|z_y - i_y| \quad (3)$$

$$\mathrm{U_z} = \delta(\psi_{\max}) - \left(\mathrm{r} - \mathrm{r}\cos(\theta_{\mathrm{ro}})\right) - \left(\mathrm{r_a} - \mathrm{r_a}\cos(\theta_{\mathrm{ra}})\right) + \left(\mathrm{Ro}(\psi) - \mathrm{Ro}(\psi)\cos(\theta_{\mathrm{Ro}})\right) + \left(\mathrm{Ro}(\psi) - \mathrm{Ro}(\psi_{\max})\right) \quad (4)$$

where z_x and z_y are the x and y-coordinates of node z, i_x and i_y are the x and y-coordinates of the applied pressure p_i, $R_o(\psi)$ is the distance from the centre of the outer ring to the outer raceway, $\delta(\psi)$ is the rigid body penetration at an angular position of ψ, $\delta(\psi_{\max})$ is the maximum rigid body penetration, r is the radius of the rolling element, θ_{ro} is the arc angle from the point of maximum rigid body penetration to another node for the rolling element at an angular position of ψ, r_a is the axial curvature of the rolling element, θ_{ra} is the angle from the point of maximum rigid body penetration to U_z and θ_{Ro} is the arc angle from the point of maximum rigid body penetration to another node on the outer.

The inverse matrix method can be used to solve the system of equations, to determine the applied pressures on the elements. If the calculated applied pressure on an element is negative, then that point is not in contact, as a negative pressure means that element is in tension. Therefore, the contact width needs to be reduced, and the applied pressures recalculated until the applied pressures are all equal to or greater than zero, where a contact force of zeros means the roller is not in contact with the raceway. For a more in-depth discussion on the contact force methodology, refer to Sayles (1996). The complete model scripts are publicly available at FigShare (Larizza et al. 2018).

4 EXPERIMENTAL METHODOLOGY

4.1 TEST CASES

The experimental test case considered in this work consisted of testing multiple defective bearings at various constant speeds and loads. The defects were machined onto the outer raceway of two ball bearings using electric discharge machining; with various arc length (β), where the machined profiles are shown in Table 1. Figure 2 shows the cross-sectional profile of the outer raceway defects. The test cases used Rexnord ER16K bearings, and Table 2 shows all critical dimensions and specifications of the bearings used. All the test bearings were run with an applied load of 500N and 600N at a shaft speed of 10 Hz. Before conducting the test, the bearing was operated for 30 minutes to ensure that the dynamic response would not change over time, due to deformations of the leading and trailing edges. To verify the model, a 0.8 mm outer raceway defect profile was simulated, to replicate the experimental testing conducted in Epps (1991)(Figure 3.2) PhD thesis. The predicted vibration response was compared to the measured experimental response collected by Epps (1991)(Figure 4.3).

Table 1: Defect profiles that were seeded onto the outer raceways of the test.

Test Bearing	Bearing Type	Arc Length (β)	Depth (μm)	Slope (α)
TB1	Ball	15.8°	100	90°
TB2	Ball	55.8°	100	90°

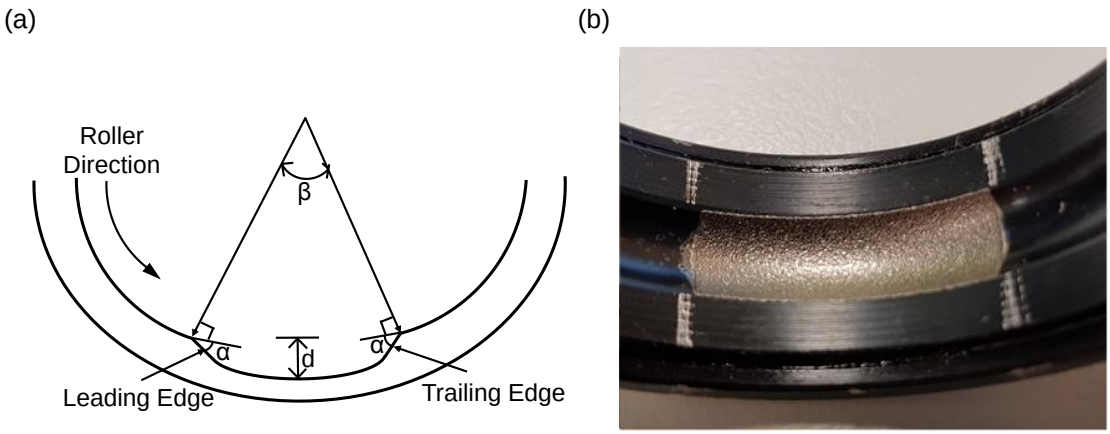

Figure 2: (a) Diagram of the defect profile in the outer ring showing the controlled defect parameters. Where α is the slope of the leading and trailing edges, β is the arc angle of the defect and d is the maximum depth of the defect. (b) Photo of the outer raceway of the ball bearing with a 55.8° long defect used in the test cases.

Table 2: Ball bearing dimensions and specifications

Parameter	Ball Value
Number of Rollers	9
Separation Angle, (°)	40
Roller Diameter, (*mm*)	7.94
Groove Diameter, (mm)	8.19
Pitch Diameter, (*mm*)	39.32

4.2 MEASURING THE VIBRATION RESPONSE OF A DEFECTIVE BEARING

Figure 3 (a) shows the modified SpectraQuest Bearing Simulator that was used to measure the dynamic response of the defective bearings. The load was applied using a hydraulic piston and measured with a load cell. A tachometer was used to measure the shaft speed. The test bearing housing has two stud-mounted accelerometers (B&K 4393) on the housing in the x and y-directions, which were used to measure the vibrations induced by the defect. Two eddy current proximity probes (mircoEpsilon eddyNCDT U05) were mounted in the x and y-directions to measure the change of the relative distance between the inner and outer rings. Figure 3 (b) shows the positions of the accelerometers and the displacement sensors used in the experiments. The data was captured using a National Instruments cDAQ system (NI cDAQ-9178 and NI-9234 modules), and MATLAB was used to record and post-process the data. The signals were acquired using a sampling frequency of 25.6 kHz. All the experimental measurement data is available at FigShare (Larizza et al. 2017).

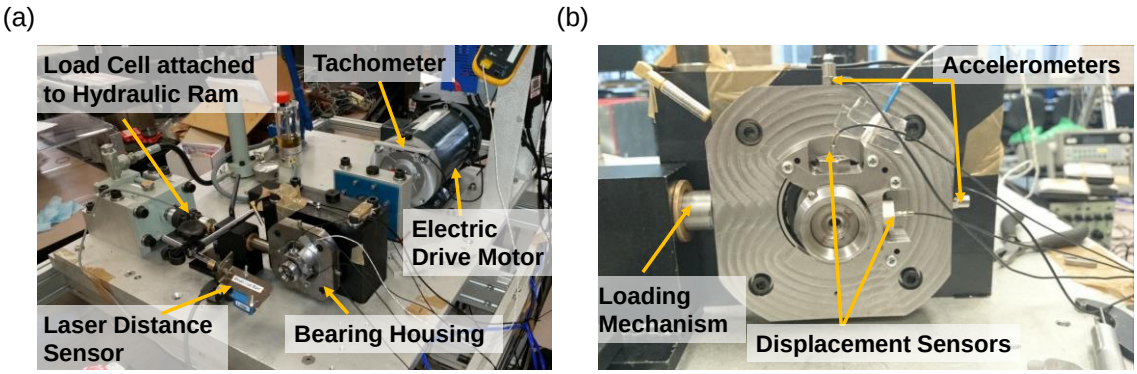

Figure 3: (a) Photo of the bearing test rig used to capture the dynamic response of a defective bearing. (b) Photo of the test bearing housing with all the measurement sensors.

5 RESULTS AND DISCUSSION

5.1 DEFECT PROFILE

The defect profile used in the model and the corresponding acceleration response of the bearing were taken from Epps (1991)(Figure 3.2 and 4.3). Epps measured the defect profile using a Rank Taylor Hobson Talysurf 10 Surface Texture Measurement Instrument. Figure 4 shows the linear trace of the 0.8 mm etched spall defect on the outer raceway of a SKF 6205 ball bearing.

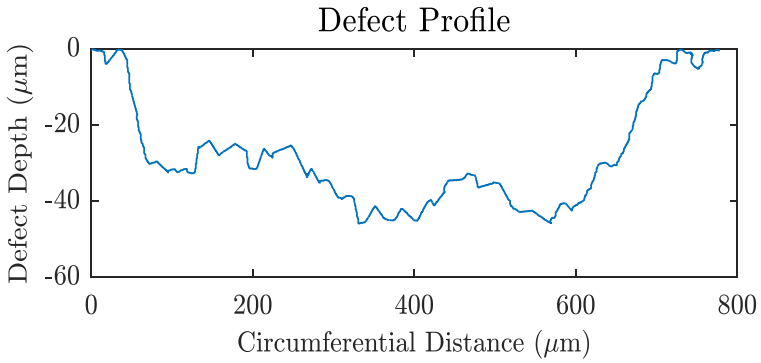

Figure 4: Defect profile of the 0.8 mm etched spall defect on the outer raceway, taken from Epps (1991)(Figure 3.2).

5.2 COMPARISON OF THE PREDICTED AND MEASURED VIBRATION RESPONSE

Figure 5 shows the comparison of the measured and predicted acceleration response of the defect, where (a) shows the measured acceleration response taken from Epps (1991)(Figure 4.3), (b) shows the predicted acceleration response, and (c) shows the predicted radial position of the rolling elements relative to the defective raceway. Where the defective bearing was tested with an applied load of 1500 N at a shaft speed of 25 Hz. When the vibration signatures from the measured vibration response of the defective bearing was compared to the predicted vibration response, the predicted results showed that when the rolling element begins to enter the defect a transient vibration response occurs (Event 1), followed by an impact response when the rolling element contact point transfers from one side to the other of the ball and begins to exit the defect (Event 2). These events occur at similar positions as the measured response. The model was able to predict the high and low-frequency vibration signature at Event 3 as the ball is forced out of the defect. The difference in the amplitudes and frequencies are caused by the estimated values of stiffness and damping coefficients of the housing and the shaft in the model, as they were not listed in Epps (1991). The damping coefficients in the model affect the decay of the predicted vibration response, and if the defect is long enough in the circumferential direction and sufficiently deep, the damping will affect the dynamics of the roller path. The profile of the defect will affect the predicted vibration response for example if the defect is longer in the circumferential direction and sufficiently deep that the rolling element completely unloads the vibration response will be similar to that presented in Figure 1. While the slope of the leading and trailing edges of the defect will cause the time take for the rolling element to entry and exit the defect to increase or decrease. The Matlab scripts are publicly available at FigShare (Larizza et al. 2018).

5.3 USING THE BEARING ASSEMBLY STIFFNESS TO DISTINGUISH LARGE DEFECTS

Referring to Figure 1, the frequency of the vibration response after the rolling element has completely unloaded (Event 2) and when the ball is being forced out of the defect (Event 4) depends on the bearing assembly stiffness. The bearing assembly stiffness can be noticeably different when an extended spall defect is present in an operational bearing, compared with a line spall defect. Figure 6 shows the spectrogram of the normalised acceleration response when an applied load of 500 N is applied to both test bearings, and when a load of 600 N is applied to TB2. All the bearings where run at a shaft speed of 10 Hz. The characteristic frequency of the entry and exit was found to be approximately 1000 Hz for the line spall defect (TB1), while for the extended spall defect the characteristic frequency was found to be 600 Hz when the applied load was 500 N.

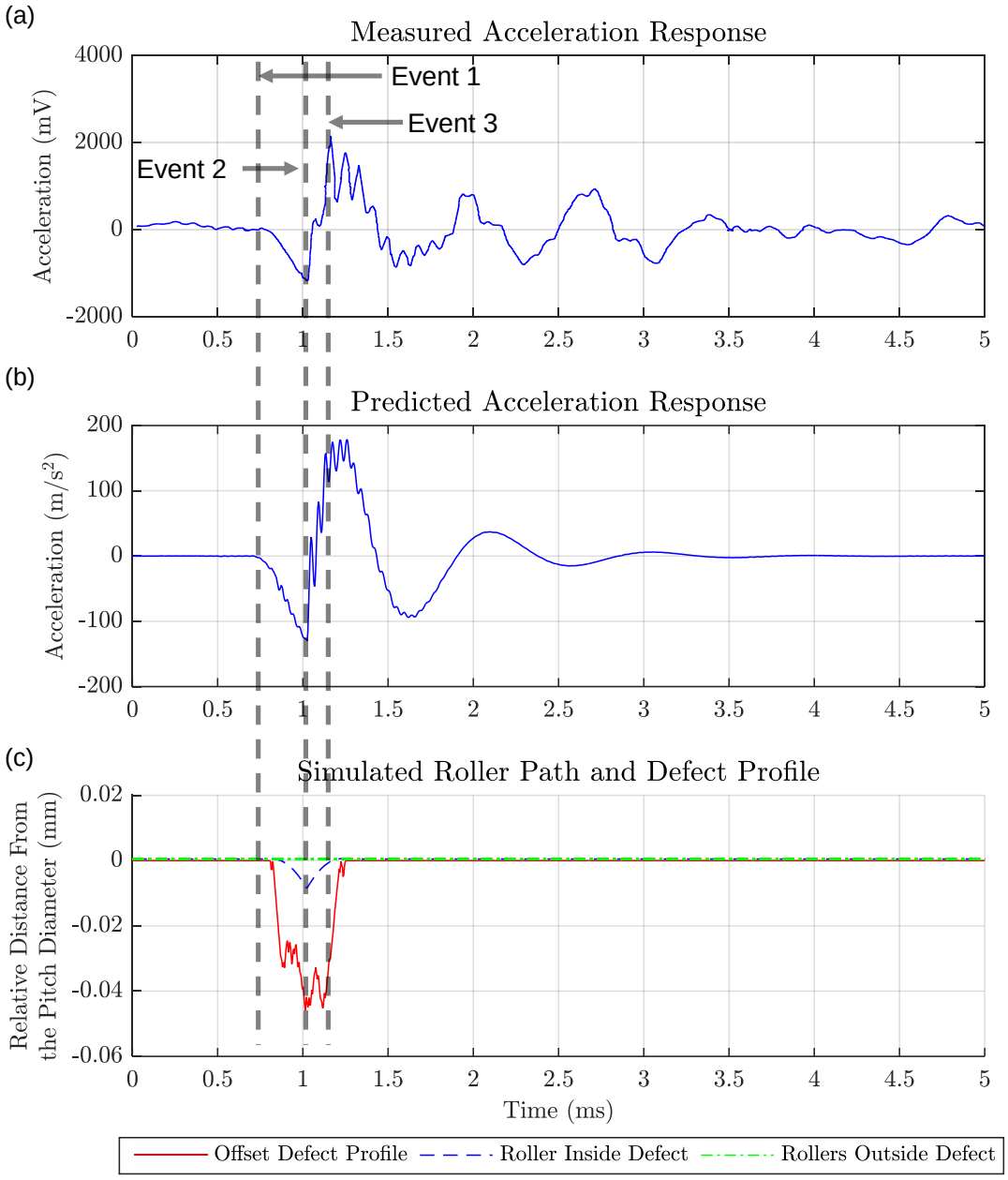

Figure 5: Comparison of the measured acceleration response of a ball bearing with a defect on the outer race-way and the simulated dynamic response with an applied load of 1500 N and a shaft speed of 25 Hz. Where, (a) is the measured acceleration signal taken from Epps (1991)(Figure 4.3), (b) is the simulated acceleration signal and (c) is the predicted roller path.

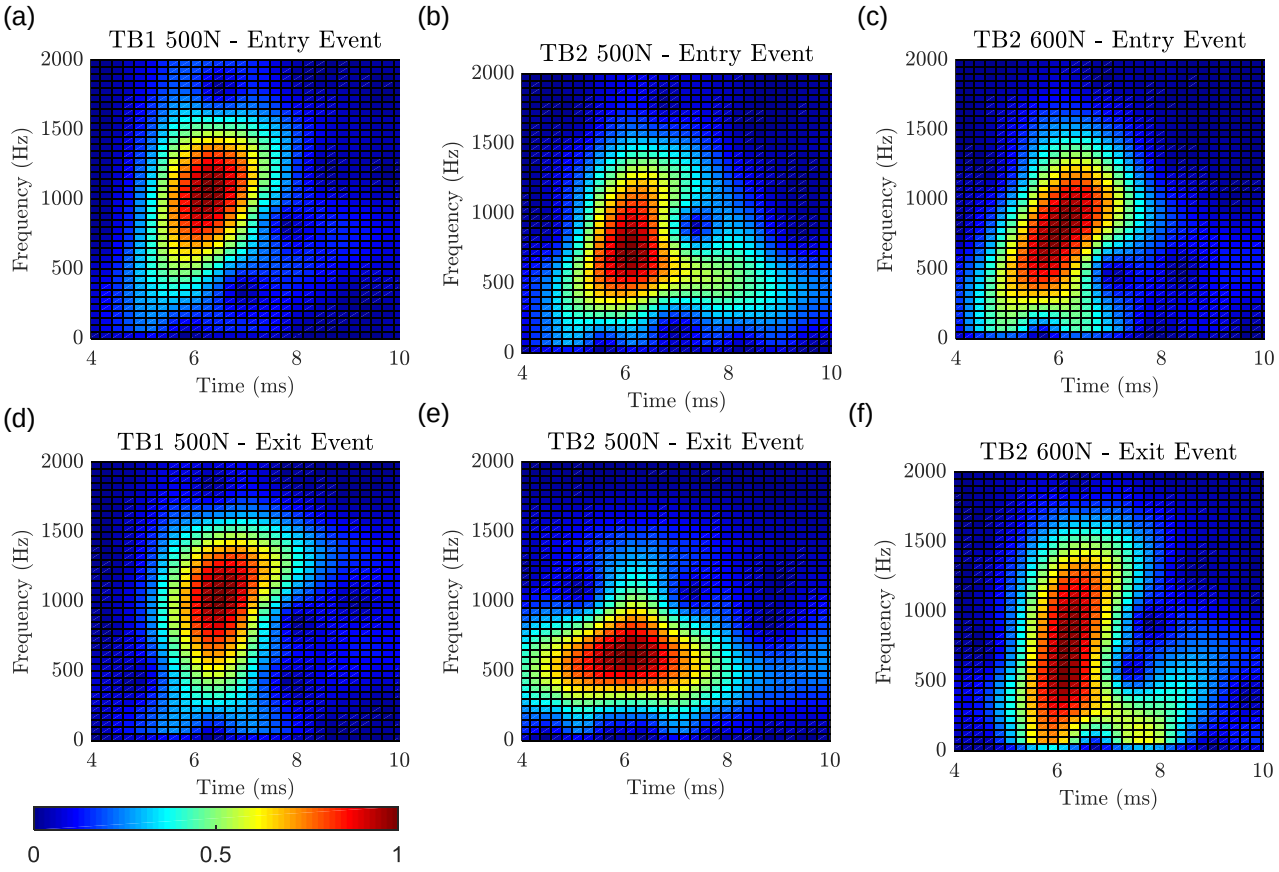

Figure 6: Spectrogram of the normalized ensemble averaged entry and exit events for TB1 and TB2 at a shaft speed of 10 Hz. Where (a) and (d) is the spectrogram for the entry and exit event of TB1 with an applied load of 500 N; (b) and (e) is the spectrogram for the entry and exit event of TB2 with an applied load of 500 N; (c) and (f) is the spectrogram for the entry and exit event of TB2 with an applied load of 600 N.

When the load is increased to 600 N, the characteristic frequency of the extended spall defect greatly increased to that of the line spall defect, as shown in Figure 6. The hypothesis presented by Petersen, Howard, and Prime (2015), can be used to determine if the size of the defect is greater than the separation angle, but the applied load must be taken into consideration, as there is a critical load when this method will not work. This critical load is when the rolling elements inside the defective region for the extended spall become loaded between the raceways, because of a high load on the bearing, causing the stiffness of the bearing assembly to sharply increase to a similar level to that of a bearing with a line spall, and causes the characteristic frequency to sharply increase.

6 CONCLUSION

This paper has demonstrated that the newly developed model can more accurately predict the vibration response of a defective bearing with a defect profile as an input into the model. It was also demonstrated that the hypothesis by Petersen, Howard, and Prime (2015) could be used to determine if a defect is greater than the separation angle of the rolling elements. Although, there is a limitation to the method as when the bearing is loaded such that the rolling elements in the defective region become loaded, the bearing assembly stiffness sharply increases to levels similar to a bearing with a line spall defect. All the experimental data is publicly available from Figshare (Larizza et al. 2017, Larizza et al. 2018).

7 ACKNOWLEDGEMENTS

The Defence Science Institute for providing funding of this research and the Australian Government for the Australian Post-Graduate Award.

8 REFERENCES

Choudhury, A., and N. Tandon. 2006. "Vibration response of rolling element bearings in a rotor bearing system to a local defect under radial load." *Journal of Tribology* 128 (2):pp. 252-261.

Epps, I.K. 1991. "An investigation into vibrations excited by discrete faults in rolling element bearings." University of Canterbury. Mechanical Engineering.

Larizza, F., C. Q. Howard, S. Grainger, and W. Wang. 2018. "Rolling Element Bearing Model Script." FigShare Accessed 1/7/2018. https://figshare.com/projects/Rolling_Element_Bearing_Model_Script/26005.

Larizza, F., A. Moazen-Ahmadi, C.Q. Howard, and S. Grainger. 2017. "The importance of bearing stiffness and load when estimating the size of a defect in a rolling element bearing." FigShare Accessed 1/7/2018. https://figshare.com/projects/The_importance_of_bearing_stiffness_and_load_when_estimating_the_size_of_a_defect_in_a_rolling_element_bearing/20612.

Mirzaei, S., T. Fahlbusch, E. Reithmeier, and G. Poll. 2008. "Experimental slip measurement of roller bearings." 2nd Ph. D. Conference AI4IA, Hannover, Germany.

Moazen-Ahmadi, A., C. Q. Howard, and D. Petersen. 2015. "The path of rolling elements in defective bearings: Observations, analysis and methods to estimate spall size." *Journal of Sound and Vibration* 366:pp. 277-292.

Moazen-Ahmadi, A., D. Petersen, and C. Q. Howard. 2015. "A nonlinear dynamic vibration model of defective bearings - The importance of modelling the finite size of rolling elements." *Mechanical Systems and Signal Processing* 53 (11):pp. 309-326.

Petersen, D., C. Q. Howard, and Z. Prime. 2015. "Varying stiffness and load distributions in defective ball bearings: Analytical formulation and application to defect size estimation." *Journal of Sound and Vibration* 337:pp. 284-300.

Sawalhi, N., and R. B. Randall. 2008a. "Simulating gear and bearing interactions in the presence of faults: Part I. The combined gear bearing dynamic model and the simulation of localised bearing faults." *Mechanical Systems and Signal Processing* 22 (8):pp. 1924-1951.

Sawalhi, N., and R. B. Randall. 2008b. "Simulating gear and bearing interactions in the presence of faults: Part II: Simulation of the vibrations produced by extended bearing faults." *Mechanical Systems and Signal Processing* 22 (8):1952-1966.

Sawalhi, N., and R. B. Randall. 2011. "Vibration response of spalled rolling element bearings: observations, simulations and signal processing techniques to track the spall size." *Mechanical Systems and Signal Processing* 25:pp. 846-870.

Sayles, R. S. 1996. "Basic principles of rough surface contact analysis using numerical methods." *Tribology International* 29 (8):639-650.

Singh, S., U. G. Kopke, C. Q. Howard, and D. Petersen. 2014. "Analyses of contact forces and vibration response for a defective rolling element bearing using an explicit dynamics finite element model." *Journal of Sound and Vibration* 333 (21):pp. 5356-5377.

Singh, S., U. Kopke, C. Q. Howard, D. Petersen, and D. Rennison. 2013. "Impact generating mechanisms in damaged rolling element bearings." *Australian Acoustical Society* 78:pp. 92-97.

Yang, Z., H. Chen, T. Yu, and B. Li. 2016. "A high-precision instrument for analyzing nonlinear dynamic behavior of bearing cage." *Review of Scientific Instruments* 87 (8):085105.